Int J Adv Manuf Technol (2016) 85:727–734
DOI 10.1007/s00170-015-7927-z

ORIGINAL ARTICLE

Internal finishing process of alumina ceramic tubes by ultrasonic-assisted magnetic abrasive finishing

H. Yun[1] **· B. Han**[1] **· Y. Chen**[1] **· M. Liao**[1]

Received: 22 June 2015 / Accepted: 1 October 2015 / Published online: 23 October 2015

Abstract This study aims to improve the efficiency and uneven texture of conventional magnetic abrasive finishing (MAF) of the inner surface of alumina ceramic tubes by changing the trajectory of a magnetic abrasive brush (MAB), presenting a new technology of ultrasonic-assisted magnetic abrasive finishing (UAMAF). The experiments compare the surface quality and material removal between MAF and UAMAF and examine the effects of workpiece speed and frequency on the surface roughness and material removal. The results show that the UAMAF has made the finishing of the inner surface of alumina ceramic tubes efficiently and precisely come true. By altering the test conditions, after 50 min processing, the processing achieves the surface roughness of R_a as fine as 0.03 μm and increases the material removal from 295 to 485 mg. The study also reveals that the frequency and workpiece speed improve the processing in varied degrees and have different finishing characteristics of the surface roughness and material removal.

Keyword Ultrasonic-assisted · Magnetic abrasive finishing · Magnetic abrasive brush · Surface roughness · Material removal

1 Introduction

Ceramics have a wide range of science application, for its high corrosion resistance and superplastic at low temperatures. Due to its hardness and brittleness, the major challenges for application, cracks, and defects are easily produced in use. The deep processing cracks will lead to local stress or even to brittle fracture. Consequently, precision machining technology of ceramics must be developed for the exploitation and application. Currently, diamond grinding is the main machining method, but its working efficiency is low, and the surface quality is worse, especially there are many grinding cracks on the surface after grinding [1, 2]. Xie studied on the high-efficiency deep grinding of silicon nitride ceramics, improving the processing efficiency and analyzing the temperature changing of grinding zones of varied processing technologies [3]. Zheng and Ma apply 1D ultrasonic grinding to ZrO_2 ceramics in order to ameliorate surface quality and suppressing the crack generation and collapse phenomenon [4–6]. Yan utilized 2D ultrasonic grinding for ZrO_2 ceramics, building motion model of abrasives of 2D ultrasonic grinding and comparing the surface quality of ultrasonic grinding with common grinding [7]. Nath et al. investigated the adverse effects of the inherent removal on the hole integrity in ultrasonic machining of structure ceramics such as entrance chipping and wall roughness [8]. Uhlmann focused on the influence of the cooling lubricant in combination with different tool specifications on the grinding of high-performance ceramics [9]. Preis et al. aimed to determine the two-body wear resistance of different dental ceramics after grinding and polishing treatments [10]. Debin Wang discussed the finishing characteristics of a magnetic field-assisted mechanochemical polishing process of Si_3N_4 fine ceramic tubes in the case of wet finishing using distilled water [11]. Yamaguchi and Shinmura presented the application of magnetic field-assisted finishing of the inner surface of alumina ceramic components, examining the effects of volume of lubricant, ferrous particle size and abrasive contact against the surface [12].

Although the characteristics of the grinding of the ceramics have been analyzed in the above references, the trajectory of vibration-assisted magnetic abrasive finishing (MAF) and the differences of the surface quality and efficiency between the

✉ H. Yun
1007372777@qq.com

[1] University of Science and Technology Liaoning, Anshan, China

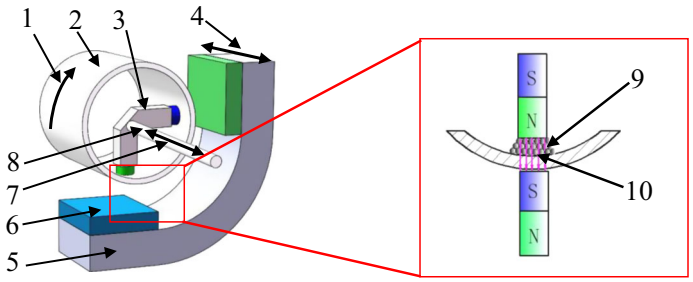

1.Tube rotation direction 2.Ceramic tube 3.V-shaped magnet 4.External magnet feeding direction 5.Magnet yoke 6.External magnet 7.Vibration direction of V-shaped magnet 8.Connecting rod 9.Magnetic abrasive brush 10.Direction of magnetic field

Fig. 1 Schematic of vibration-assisted magnetic abrasive finishing. 1. Tube rotation, 2. Ceramic tube, 3. V-shaped magnet, 4. External magnet feeding direction, 5. Magnet yoke, 6. External magnet, 7. Vibration direction of V-shaped magnet, 8. Connecting rod, 9. Magnetic abrasive brush, 10. Direction of magnetic field

ultrasonic-assisted MAF (UAMAF) and MAF are seldom reported. The study simulates the trajectory of different frequency and workpiece speed, deeply analyzing the influence of varied trajectories on the efficiency and surface quality. The experiments compare the surface roughness, material removal, and the micromorphology between UAMAF and MAF and examine the effects of workpiece speed and frequency on the surface roughness and material removal. This study provides a new technology of internal finishing for precision ceramics.

1.1 Theoretical analysis

1.1.1 Processing principle

The UAMAF is based on the MAF, which is accompanied with ultrasonic vibration in the processing. The advantage of the UAMAF is low finishing force, high accuracy, high efficiency and good surface integrity, due to its special machining trajectory and the effect of ultrasonic vibration. Figure 1 shows a schematic of vibration-assisted magnetic abrasive finishing of the inner surface of alumina tubes. A V-shaped magnet with magnetic abrasive particles (MAPs) is placed inside the ceramic tube, which forms the magnetic circuit with the external magnetic poles. The MAPs are conglomerated along the magnetic field direction to condense into the magnetic abrasive brush (MAB), sandwiched between the inner surface of the tube and the V-shaped magnet to increase the magnetic force acting on the MAPs [13–19]. The workpiece rotates at high speed, and the external magnet is reciprocating feeding along the ceramic tube axis, which drives the movement of a V-shaped magnet along the tube axis. At the same time, ultrasonic vibration with certain amplitude and frequency is adherent to the V-shaped magnet. The ultrasonic power generates high-frequency electrical signals that are supplied to the piezoelectric crystals within the transducer. The high-frequency electrical signals of 20 kHz are converted to mechanical vibrations by the transducer [20, 21]. The amplitude achievable from the transducer does not exceed 3 to 5 μm. Hence, the amplitude is amplified by the concentrator and then transmitted to the V-shaped magnet by the connecting rod linking with the concentrator to improve the trajectory of MAB.

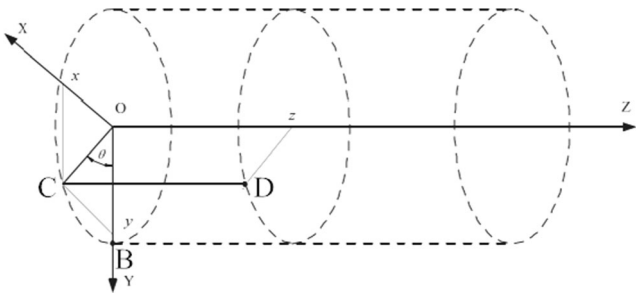

Fig. 2 Position relationship between the MAB and workpiece

Figure 2 shows the position relationship between the MAB and workpiece. Assume that the workpiece is fixed and the initial position of the MAB is at B. The motion of the MAB consists of three kinds of speeds: rotating motion relative to the workpiece, feeding motion of Z axis, and vibration motion of Z axis. The MAB moves from B to D with the time t. The coordinates of the MAB at point D is:

$$\begin{cases} x = R\sin\theta = R\sin\omega_L t \\ y = R\cos\theta = R\cos\omega_L t \\ z = V_L\omega_L t\big/2\pi + A\sin 2\pi ft \end{cases} \quad (1)$$

x,y,z—coordinate of point D, mm
R—radius of workpiece, mm
Θ—rotating angle of the MAB, rad
ω_L—relative angular speed, rad/s
V_L—speed of axial feeding,mm/r
f—frequency, Hz
A–amplitude, mm

1.1.2 Simulation of trajectory of the MAB

The actual process is made up by a workpiece rotating in high speed, and the MAB feeding accompanied by vibrating in the direction of the workpiece axis. In order to simplify simulation, the motion model is assumed as workpiece rotating accompanied by feeding along the workpiece axis, and the MAB vibrating in the direction of workpiece axis. Based on the

above assumption, the trajectory of the MAB will be analyzed.

Effects of frequency on trajectory of the MAB Set process parameters as this: workpiece speed of 1000 r/min, feeding speed of 2 mm/s, and amplitude of 5 mm. Simulate the trajectory of the MAB in 3 s with varied frequencies. Figure 3a shows the trajectory of MAF. The reciprocating motion of MAF is only formed by feeding motion. The trajectory of MAF is continuous, causing to small arc cutting, the length of which is short and the shape of which is too regular to interfere with each other. Because of the regular trajectory, the generation path of cracks of MAF is too long, and the area is too large, leading to poor surface quality. The reciprocating motion of UAMAF is formed by feeding motion mixed with axial vibration. The trajectory becomes longer and wider than which of the MAF because of the ultrasonic vibration, enhancing the interference among the trajectory of the MAB and forming micronization cutting. The trajectory interferes strongly leading to cutting path shortly and chipping shortly, and a better surface quality is achieved. The special trajectory forms a huge net on the surface of the workpiece, and the denser the net is, the higher the efficiency is. The trajectory varies with the frequency of the vibration and the workpiece speed. Under the condition of workpiece speed stability, when the frequency of vibration is less than the frequency of workpiece speed, the helix intersects with a great angle as shown in Fig. 3b, which is not conductive to improve the surface quality. As the frequency of vibration is increasing, the angle of helix intersection is gradually decreased, and the size of the non-removal traces on the surface is reduced as shown in Fig. 3c. The vibration of high frequency can completely interfere with the trajectory of the MAB and completely get rid of the non-removal traces as shown in Fig. 3d. Thus, when the frequency of workpiece speed is less than the frequency of the vibration, the surface quality and the efficiency can both improve.

Effects of workpiece speed on trajectory of the MAB Set process parameters as this: amplitude of 5 mm, feeding speed of 2 mm/s, and frequency of 30 Hz. Simulate the trajectory of the MAB in 3 s with varied workpiece speeds. Figure 4a shows when the workpiece speed is low, the trajectory is sparse, and the efficiency is low, and the non-removal traces are obviously seen. The intersection point of trajectory is easy to cause edge-breaking, leading to poor surface quality. With the gradual increase of the workpiece speed, relative to the workpiece, the kinetic energy of the MAPs is increased. The

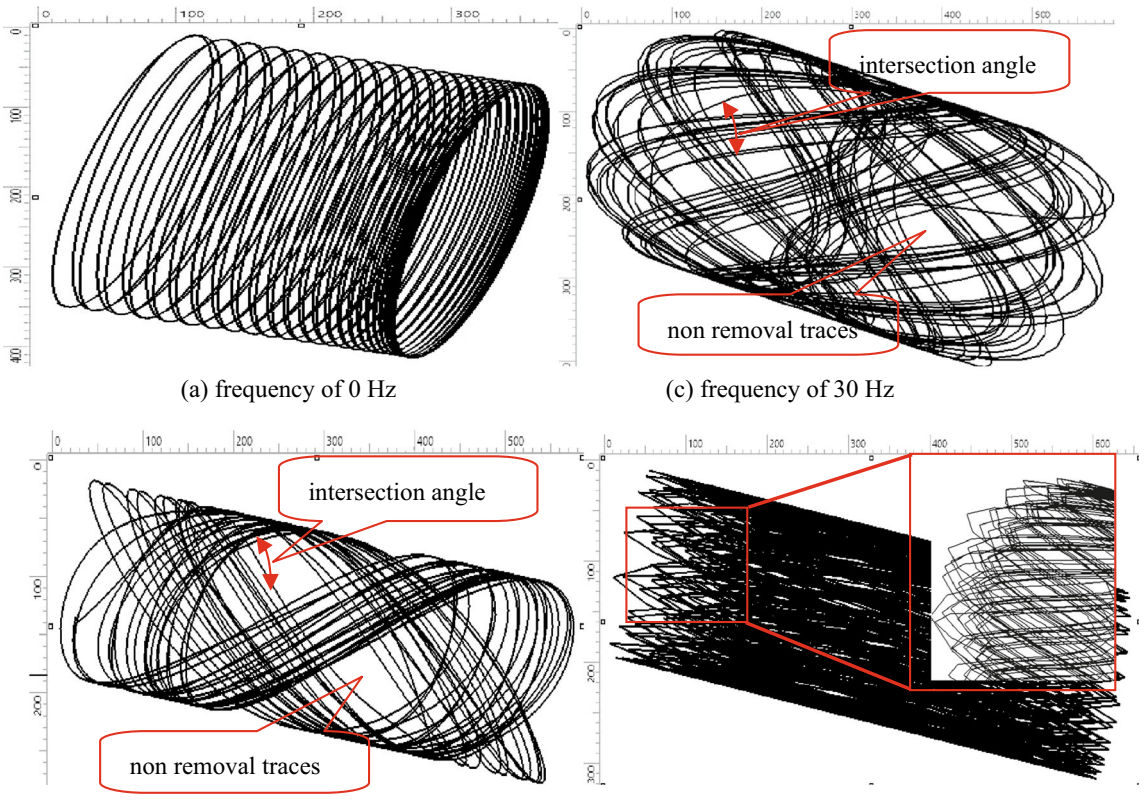

(a) frequency of 0 Hz (c) frequency of 30 Hz

(b) frequency of 10 Hz (d) Trajectory of frequency of 80 Hz

Fig. 3 Effects of frequency on the MAB trajectory; **a** frequency of 0 Hz, **b** frequency of 10 Hz, **c** frequency of 30 Hz, and **d** frequency of 80 Hz

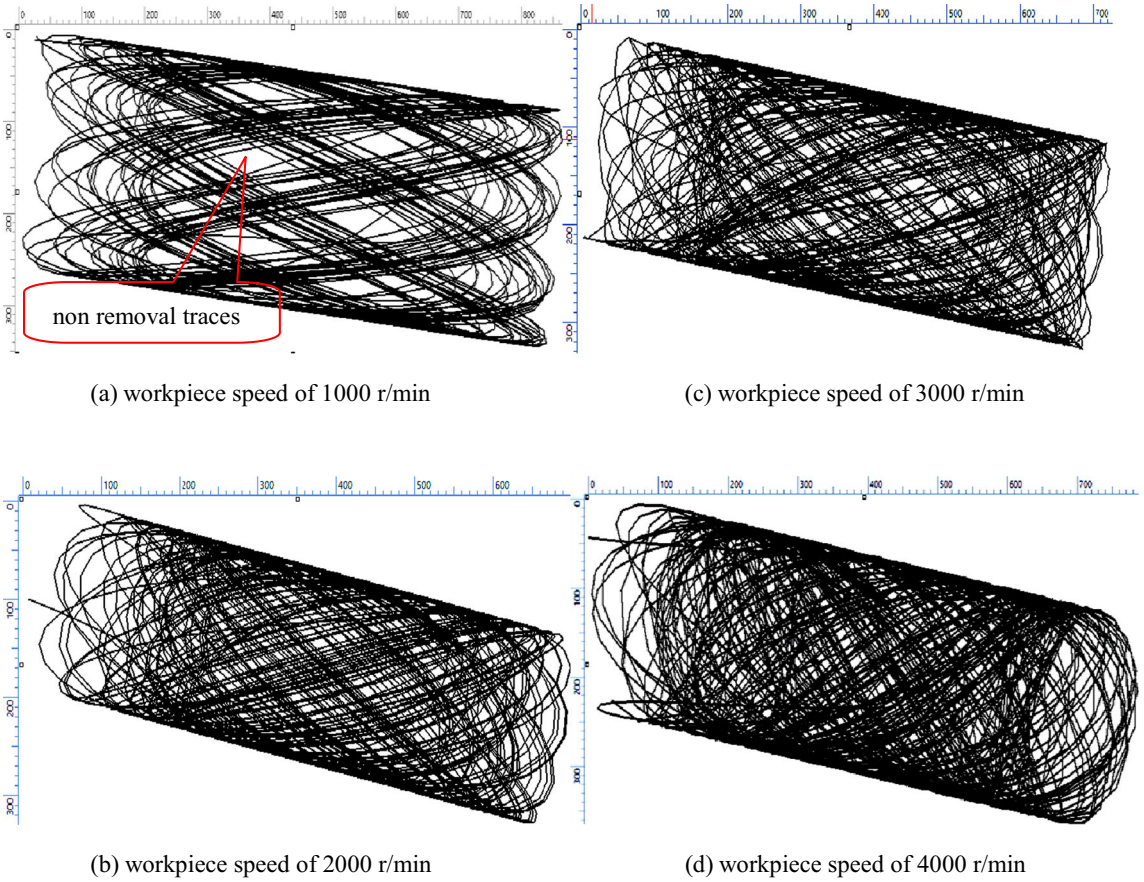

Fig. 4 Effects of workpiece speed on the MAB; **a** workpiece speed of 1000 r/min, **b** workpiece speed of 2000 r/min, **c** workpiece speed of 3000 r/min, and **d** workpiece speed of 4000 r/min

friction between the workpiece and the MAPs greatly intensifies, and the utilization ratio of the MAPs is improved. The trajectory becomes more intensive, and the interference of the trajectory is stronger as shown in Fig. 4b, leading to a high efficiency. The workpiece speed has a great effect on the deformation of workpiece of the material removal, and impacts little on the surface roughness, because the frequency of vibration is much higher than the frequency of workpiece speed. As the workpiece speeds further up, the trajectory becomes disordered, and the vibration effects are reduced as shown in Fig. 4c. The surface roughness and the temperature of finishing zones have a tendency to increase. When the workpiece speed is too high, the finishing zone is full of traces, causing the surface quality down as shown in Fig. 4d. On the other hand, a workpiece rotating in a too high speed will make the stability of the mechanism down, further letting the surface roughness down. Hence, under the premise of ensuring the processing quality, the workpiece speed is as high as possible.

1.2 Experimental conditions and device

The surface roughness of R_a is performed with a surface roughness profile tester. The material removal of Δm is measured on an electronic force balance with 0.01 mg resolution. The surface is microscopically examined using 3D optical microscope. The experiments are halted every 10 min to measure the surface roughness and the material removal. The abrasive is renewed every 10 min. Figure 5 shows the external view of the experimental device. Table 1 shows mechanical and physical properties of alumina ceramic tubes, and Table 2 shows the test conditions.

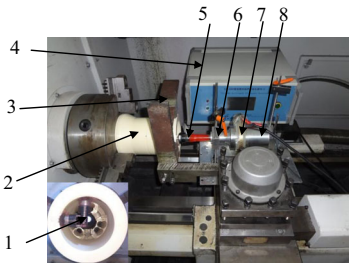

1.V-shape magnet2.Ceramic tube3.Magnetic yoke4.Ultrasonic power5.Collect 6.Amplitude transformer7.Slip ring8.Transducer

Fig. 5 The UAMAF device. 1. V-shape magnet, 2. Ceramic tube, 3. Magnetic yoke, 4. Ultrasonic power, 5. Collect, 6. Amplitude transformer, 7. Slip ring, 8. Transducer

Table 1 Mechanical and physical properties of alumina ceramic tubes

Title	Parameter
Moths hardness	9
Content of alumina	≥99.3 %
Tensile strength	3160 kg/cm^2
Flexural strength	2520 kg/cm^2
Volume density	>3.8 g/cm^3

1.3 Experimental results

1.3.1 Effects of ultrasonic vibration on surface roughness and material removal

The inner surface of an alumina ceramic tube is finished by MAF and UAMAF. The workpiece speed is 2000 r/min, and the frequency of vibration is 19 kHz. The other test conditions are the same as those listed in Table 2. Figure 6 shows the surface roughness and material removal with finishing time of MAF and UAMAF. It can be seen that the surface roughness and material removal of MAF are all worse than which of UAMAF. After finishing for 50 min, the surface roughness of MAF falls from 1.1 to 0.55 μm, and the material removal is 295 mg. The surface roughness of UAMAF falls from 1.12 to 0.03 μm, and the material removal is 485 mg. The reason is that the UAMAF makes the friction between the MAPs and the workpiece enhanced and promotes the kinetic energy of the MAPs. Because of this, the material removal is greatly increased. On the other hand, the vibration of high frequency has a better influence on the interference of the trajectory, which makes the size of non-removal traces smaller, getting a smooth trajectory, and obviously improving the surface quality.

1.3.2 Effects of ultrasonic vibration on the micromorphology

It has great differences of the micromorphology between MAF and UAMAF. Figure 7 shows the surface micromorphology of MAF and UAMAF after finishing for 50 min. The finishing surface of MAF is made up of brittle fracture zone and scrape and extrusion zone. The brittle fracture zone has no finishing

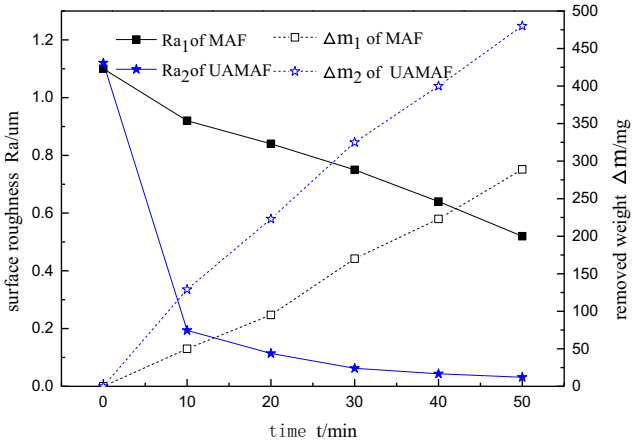

Fig. 6 Surface roughness and material removal with finishing time of MAF and UAMAF

traces, and the edge of it is broken. The scrape and extrusion zone has little finishing traces, and the traces of plastic deformation are narrow and deep. It can be seen that in Fig. 7a, the 3D micromorphology of MAF is so uneven that the altitude differences between the peaks and troughs are large, which is about 80 μm. The grooves are unequal in the width and depth. There are many marks of brittle fracture on the finishing zones in Fig. 7b,which are continuous. The traces are discontinuous and irregular, and the materials are flake-off, which are removed in fragile mode, and only local parts have scrape and extrusion phenomenons. The surface quality is bad.

The finishing surface of UAMAF is made up of brittle fracture zone and plastic working zone, but the area of the brittle fracture zone is much smaller than which of MAF. The traces in the plastic working zone are like metal grinding, and look so smooth and straight. The edge of traces in the plastic working zone can be seen as a small plastic bulge. The 3D micromorphology of UAMAF in Fig. 7c shows that the finishing surface of UAMAF is so smooth that the altitude differences between the peaks and troughs greatly reduced ,which is about 10 μm. The finishing grooves of UAMAF are almost equal in width and depth. The traces on the surface cross with each other, which looks like a water pattern in Fig. 7d. The distribution of the traces is uniform and continuous. There are

Table 2 Test conditions

Title	Parameter
Workpiece	Alumina ceramic tube Φ50×100 mm
Magnet	Permanent magnet 40×20×10 mm and 10×10×5 mm
Abrasive materials	Iron powder of 150 μm and diamond paste of W2.5
Grinding fluid	Oil-based lubricant of 5 ml
Feeding speed	2 mm/s
Workpiece speed	600, 1000, 1500, 2000 r/min
Frequency of UAMAF	0, 12, 15, 19 kHz

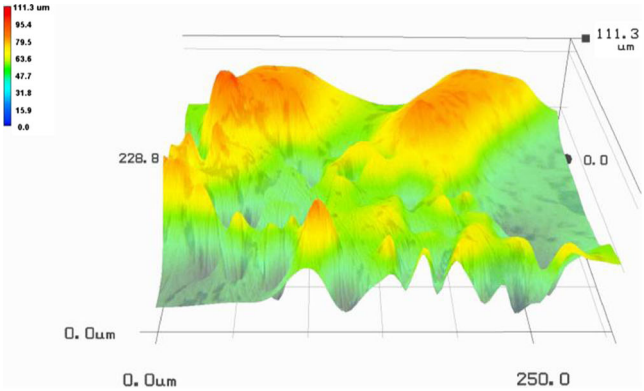

(a) 3D micromorphology of MAF

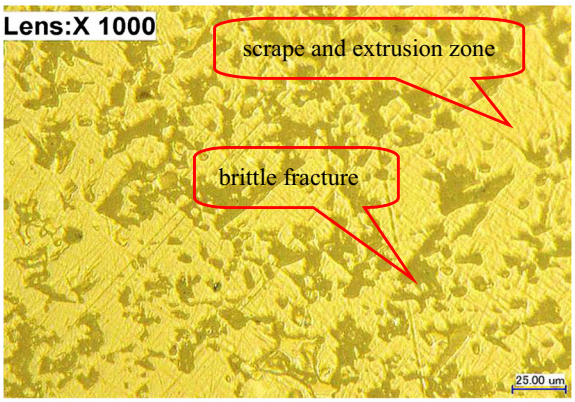

(b) the micromorphology of MAF

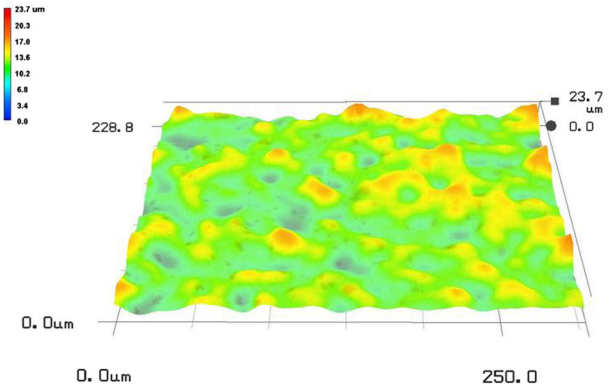

(c) 3D micromorphology of UAMAF

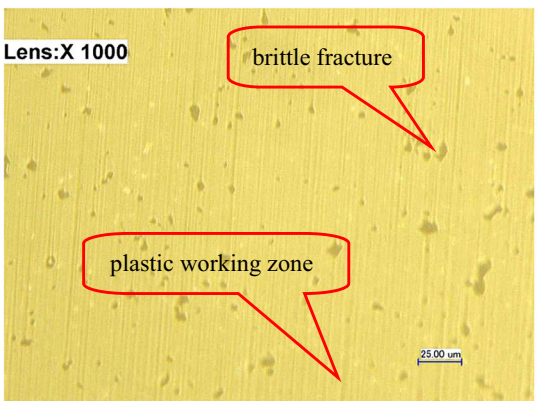

(d) the micromorphology of UAMAF

◀ **Fig. 7** The micromorphology of MAF and UAMAF; **a** 3D micromorphology of MAF, **b** the micromorphology of MAF, **c** 3D micromorphology of UAMAF, and **d** the micromorphology of UAMAF

obvious marks of plastic working traces on the surface after UAMAF. The materials are removed almost in plastic mode, and the surface has good integrity [7, 20].

There are mainly two reasons for the phenomenons. Firstly, the trajectory of the MAB has been changed, causing the removal mechanism to be improved. The traces form a network on the finishing zones. The denser the network is, the lower the surface roughness is. Secondly, the ultrasonic vibration keeps the sharpness of the MAPs, reducing the mean finishing force, which may reduce the generation of the fracture on the surface, and expands the plastic working zone of the materials, leading to a fine surface.

1.3.3 Effects of ultrasonic vibration on the surface roughness profile

Figure 8a shows the unevenness of the surface after MAF. If the size of the diamond abrasive is smaller than the width of the valleys on the surface, it can reach into the valleys. While the width of the valley is about 30 μm as shown in Fig. 8a, the size of the diamond abrasive is about 2.5 μm, and it could reach into the valleys. However, the diamond abrasive applies only the minimal force, unless it is pressed on the surface by the iron particles. The mean diameter of the iron particles is about 100 μm, which cannot reach into the valleys. Because of the lack of finishing force, the diamond abrasive inside the valley could not remove enough material for finishing. So, the surface quality is poor. The surface roughness profile of UAMAF is very flat. The ultrasonic vibration increases the kinetic energy of the diamond abrasive, and the valleys will soon become flat. The size of diamond abrasive is too large to reach into the valley. Consequently, only the diamond abrasive sandwiched between the peaks of the surface and the iron particles could result in efficient finishing performance with minimum material removal. On the other hand, the material removal of MAF is almost in fragile mode, whose surface has lots of brittle fracture zones, leading to poor surface quality. But the material removal of UAMAF is almost in plastic mode, whose surface has good integrity. So, the contour curve of UAMAF is very flat.

1.3.4 Effects of frequency on surface roughness and material removal

The workpiece speed is 2000 r/min, and the other test conditions are shown in Table 2. The higher the frequency is, the smoother the surface is, and the larger the material removal is. The increase of the frequency must sustain the relative motion of the MAPs for the material removal, generating the

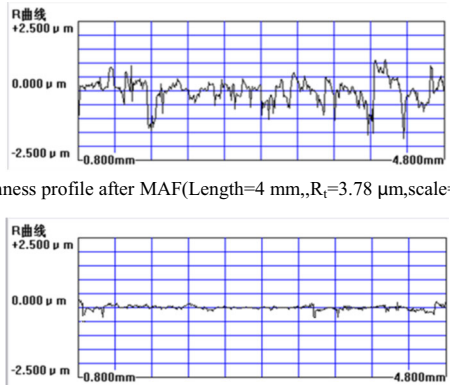

(a) The surface roughness profile after MAF(Length=4 mm,,R_t=3.78 μm,scale=5 mm,R_a=0.55 μm)

(b) The surface roughness profile after UAMAF(Length=4 mm, R_t=1.78 μm,scale=5 mm、R_a=0.03 μm)

Fig. 8 The surface roughness profile of MAF and UAMAF. **a** The surface roughness profile after MAF (length=4 mm, R_t= 3.78 μm, scale=5 mm, R_a= 0.55 μm). **b** The surface roughness profile after UAMAF (length=4 mm, R_t=1.78 μm, scale=5 mm, R_a=0.03 μm)

smoothly surface in a short time. As shown in Fig. 9, after finishing for 50 min, the surface roughness of MAF falls from 1.1 to 0.55 μm, and the material removal is 295 mg. As the frequency goes up, after finishing for 30 min of low frequency of 12 kHz, the surface roughness falls slowly, not fitting for the precision machining. When the frequency increases to 19 kHz, after finishing for 50 min, the surface roughness falls to 0.03 μm, and the material removal increases by 190 mg. This is because the low-frequency vibration has a bad influence on the interference of the trajectory, which causes to a long generation path of cracks and a large area of material removal. The kinetic energy of the MAPs is low. So, the surface quality is worse and the efficiency is lower. As the frequency goes up, the size of non-removal traces obviously reduces and cuts down the generation path of cracks. The high frequency produces multi-level cracks, and the cracks will be removed before fully generating. It is good for material to be removed in plastic mode. At the same time, vibration of high frequency can contribute to material breaking to the workpiece surface, greatly improving the material removal.

1.3.5 Effects of workpiece speed on surface roughness and material removal

The frequency is 19 kHz, and the other test conditions are shown in Table 2. As shown in Fig. 10, the workpiece speed plays a significant role in the material removal but has little influence on the surface roughness. When the workpiece speed is 600 r/min, the surface roughness falls from 1.1 to 0.09 μm, and the material removal is 310 mg. With the workpiece speed increasing to 2000 r/min, the surface roughness is better than which of 600 r/min, and the material removal becomes larger. The best surface roughness is 0.03 μm and the largest material is 485 mg. The reason is that when the workpiece speed is low, the trajectory is sparse, resulting in a low efficiency, and the non-removal traces are obviously seen, leading to a bad surface quality.

As the workpiece speeds further up, the processing distance of the MAPs in unit time is promoted and the utilization ratio of the MAPs is improved, making the material removal increase greatly. With the workpiece increasing in speed, the

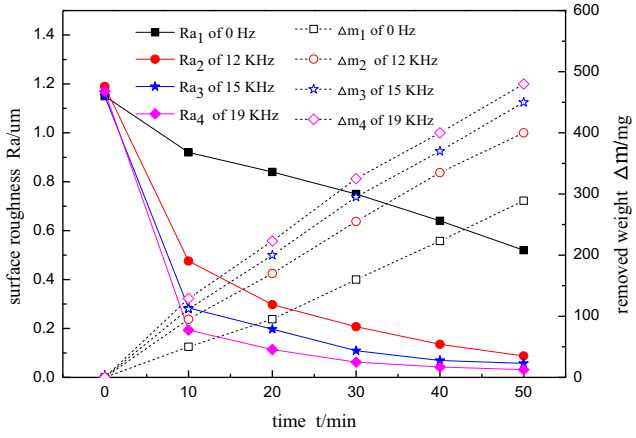

Fig. 9 Surface roughness and material removal with finishing time of varied frequency

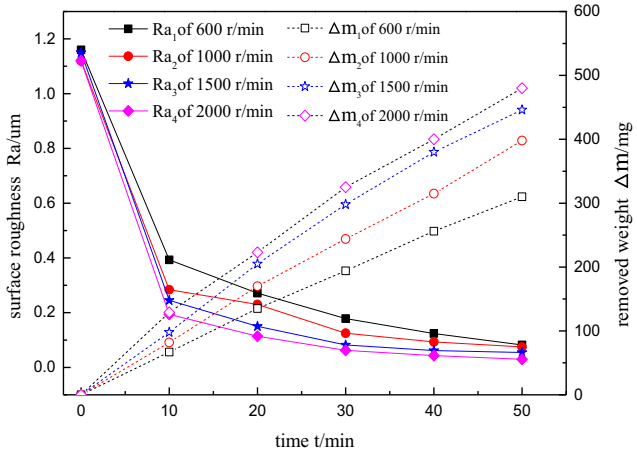

Fig. 10 Surface roughness and material removal with finishing time of varied workpiece speed

interference of the trajectory of the MAB strengthens. But the frequency of vibration is much higher than the frequency of workpiece speed, the workpiece speed has little impact on the intersection angle, leading to little influence on the surface roughness.

2 Conclusions

The results of the study can be summarized as follows:

(1) Comparing the UAMAF with the MAF, the material removal and the surface roughness are greatly improved, as the revolution of the finishing trajectory. After finishing for 50 min, the surface roughness of UAMAF falls from 1.1 to 0.03 μm, and the material removal is 485 mg, and the area of brittle fracture is much smaller than which of MAF.

(2) The surface roughness and material removal are all related to the frequency. When the frequency varies from 0 to 19 kHz, the higher the frequency is, the better the surface quality is, and the larger the material removal is. After finishing for 50 min, the best surface roughness is 0.03 μm, and the largest material removal is 485 mg.

(3) The workpiece speed plays a significant role in the material removal, but has little influence on the surface roughness. When the workpiece speed is 600 r/min, the surface roughness falls from 1.1 to 0.09 μm, and the material removal is 310 mg. With the workpiece speed increasing to 2000 r/min, the surface roughness falls to 0.03 μm, and the material removal increased by 175 mg.

References

1. Xiao Q (2011) Research on the material removal rates and surface features of SiC single crystal by ultrasonic polishing. J Synthetic Crystals 43(2):496–499
2. Cheng J, Gong YD, Yan XQ (2013) Modeling and experimental study of complex critical condition for ductile-regime micro-grinding of hard brittle material. J Mech Eng 49(23):191–198
3. Xie GZ, Huang H, Xu XP, Huang HW (2009) Study on the temperature in the high efficiency deep grinding of silicon nitride. J Mech Eng 45(3):293–297
4. Zheng K, Xiao XZ, Liao WH (2014) Test for ultrasonic vibration assisted grinding of sintered zirconia ceramics crowns. J Vibration AShock 33(4):32–36
5. Zheng K, Xiao XZ, Liao WH (2013) Study on rotary ultrasonic machining of sintered zirconia dental ceramics. J Synthetic Crystals 42(9):1865–1869
6. Ma H, Zhao B, Xie P (2010) Research on relation between ultrasonic grinding frequencies and surface quality for Al_2O_3-ZrO_2 nano-composite ceramics. J Shanghai Jiao Tong Univ 44(12): 1763–1766
7. Yan YY, Zhao B, Liu JL (2009) Ultraprecision surface finishing of nano-ZrO_2 ceramics using two-dimensional ultrasonic-assisted grinding. Int J Adv Manuf technol 43:462–467
8. Nath C, Lim GC, Zheng HY (2012) Influence of the material removal mechanisms on hole integrity in ultrasonic machining of structural ceramics. Ultrasonics 52:605–613
9. Uhlmann E, Sammler C (2010) Influence of coolant conditions in ultrasonic-assisted grinding of high-performance ceramics. Prod Process 4:581–587
10. Preis V, Behr M, Handel G, Schneider FS, Hahnel S, Rosenrtitt M (2012) Wear performance of dental ceramics after grinding and polishing treatments. J Mech Behav Biomed Mater 10:13–22
11. Wang D, Shinmura T, Yamaguchi H (2004) Study of magnetic field assisted mechanochemical polishing process for inner surface of Si_3N_4 ceramic components finishing characteristics under wet finishing using distilled water. Machine tools and manufacture., pp 1547–1553
12. Yamaguchi H, Shinmura T (2004) Internal finishing for alumina ceramic components by a magnetic field-assisted finishing process. Precis Eng 28:135–142
13. Chen Y, Zhang YM, Deng C (2014) Application of V-shaped magnet in polishing the inner surface of the SU304 tubing. J Mech Eng 2014(15):187–191
14. Chen Y, Liu ZQ, Wang XK (2013) Ultrasonic vibration-assisted magnetic abrasive finishing. Trans Chin Soc Agric Machinery 44(10):295–297
15. Han B, Deng C, Chen Y (2013) The spherical processing of inner surface of bending pipe by magnetic abrasive finishing. Tribology 33(6):566–570
16. Lu YP, Ma J, Cai JW (2006) Study of intelligent control system in magnetic abrasive finishing on molds free surface process. Trans Chin Soc Agric Machinery 37(10):164–168
17. Liu ZQ, Chen Y, Li YJ, Zhang X (2013) Comprehensive performance evaluation of the magnetic abrasive particles. Int J Adv Manuf Technol 68:631–640
18. Jayswal SC, Jain VK, Dixit PM (2005) Modeling and simulation of magnetic abrasive finishing process. Int J Adv Manuf Technol 26: 477–490
19. Lee YH, Wu KL, Bai CT, Liao CY, Yan BH (2014) Planetary motion combined with two-dimensional vibration-assisted magnetic abrasive finishing. Int J Adv Manuf Technol 34:122–130
20. Zhang HL, Zhang JH (2010) Brittle material removal mechanism of ultrasonic vibration-assisted grinding. J Chongqing Univ 33(10): 33–37
21. Mulik RS, Pandey PM (2010) Mechanism of surface finishing in ultrasonic-assisted magnetic abrasive finishing. Mater Manuf Processes 25:1418–1427